Numerical Simulation of the SGEMP Inside a Target Chamber of a Laser Inertial Confinement Facility

Meng Cui, Xu Zhiqian, Jiang Yunsheng, Zheng Wanguo, and Dang Zhao, *Member, IEEE*

***Abstract*— After X-ray irradiate a metal cavity, a large number of photoelectrons are emitted into the internal space, thereby producing a very strong system-generated electromagnetic pulse (SGEMP). The X-ray environment inside a laser inertial confinement device is very complex. Even if the diagnostic equipment working inside the target chamber has a good electromagnetic shielding capability, it would still face severe SGEMP interference. In this paper, the X-ray environments inside target chambers of National Ignition Facility, optimized method for estimated guidance accuracy (OMEGA), and Shenguang-III (SG-III) facility were obtained through a survey of the literature. In light of the survey results, the time-biased finite-difference time-domain method and the particle-in-cell method were used to numerically simulate SGEMP inside a 2-D cylindrical cavity model. Besides, the relationships between the SGEMP in the cavity and parameters such as X-ray fluence, energy spectrum, pulsewidth, and spatial size of the model were studied. The fluence and pulsewidth of the X-ray were found to have a more significant effect on the time-domain waveform of the electromagnetic field. Finally, based on the calculation results, the SGEMP of the SG-III facility in the target chamber was calculated to approximately be 0.75 MV/m.**

***Index Terms*— Inertial confinement fusion (ICF), particle-in-cell (PIC) particle simulation, radiation environment, system-generated electromagnetic pulse (SGEMP).**

I. Introduction

LASER inertial confinement fusion (ICF) is a method for achieving thermonuclear fusion by using the energy from a megajoule-class pulsed laser as a driving source to compress the deuterium and tritium fuels in the target pellet via implosion. Currently, the U.S., France, China, and Japan have established high-power laser ICF devices.

When X-rays irradiate the surface of a metal shell, large number of photoelectrons would be emitted toward the internal cavity. These free electrons have a certain energy and angular distribution. The movement of the electrons forms a spatial current, which self-consistently excites a very strong, transient electromagnetic field. This type of electromagnetic field, which is completely generated by the system's own electrons, is called a system-generated electromagnetic pulse (SGEMP). In the 1970s, countries outside China began to study SGEMP interference experienced by the missiles and satellite systems in a high-altitude nuclear environment, and China also launched some relevant studies. Since nuclear testing has been banned internationally and SGEMP simulation experiments using dense plasma focus devices, modified relativistic electron beams, or current injection as well as other methods have been very difficult to implement because of the restriction to low X-ray fluence, high requirements for the vacuum environment, great signal interference as well as other factors [1], [2], numerical simulation has become the main means for studying SGEMP. Woods *et al.* established many types of cavity models. They used the Arbitrary Body of Revolution Code program to conduct a large number of numerical calculations. They explored the effects of X-ray fluence, energy spectrum, pulsewidth, cavity gas pressure, and other parameters on the SGEMP time-domain response. Woods *et al.* found that the peak field strength could reach several MV/m [3]–[5]. Researchers at the Northwest Institute of Nuclear Technology calculated the SGEMP response on aircrafts to exceed 5 MV/m, which is generated by the pulsed X-rays released in a nuclear explosion [6], [7].

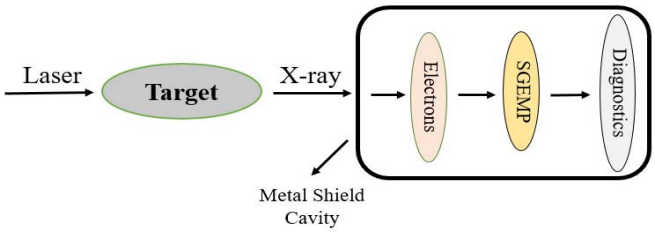

Fig. 1. Diagram of the generation of SGEMP inside a target chamber.

In shooting experiments with laser inertial confinement devices, researchers found the phenomenon of electromagnetic interference even if the equipment in the target chamber was designed with electromagnetic shielding. As illustrated in Fig. 1, after a shooting, the target is compressed and an implosion occurs, accompanied by many secondary effects, generating high-power electromagnetic pulse, and X-ray. Therefore, a metal shielding layer used outside the diagnostics

Manuscript received July 18, 2017; revised August 1, 2017 and August 11, 2017; accepted August 12, 2017. Date of publication August 17, 2017; date of current version October 17, 2017.

M. Cui, X. Zhiqian, and J. Yunsheng are with the Department of Engineering Physics, Tsinghua University, Beijing 100084, China, and also with the Key Laboratory of Particle & Radiation Imaging, Ministry of Education, Beijing 100084, China, (e-mail: mengcuir@tsinghua.edu.cn; zq-xu13@mails.tsinghua.edu.cn; jys16@mails.tsinghua.edu.cn).

Z. Wanguo and D. Zhao are with the Research Center of Laser Fusion, CAEP, Mianyang 621900,China, (e-mail: wgzheng_caep@sina.com; qingzhaodang@163.com).

Color versions of one or more of the figures in this paper are available online at http://ieeexplore.ieee.org.

Digital Object Identifier 10.1109/TNS.2017.2740930

TABLE I
X-RAY ENVIRONMENT OF THE OMEGA DEVICE

Target	Laser Power (W/cm^2)	Pulse Width (ns)	Energy Band (keV)	X-ray Yield (J/sr)
Ar	-	2	3-3.6 2-5.5	55.6 ± 24.3 64.7 ± 14.3
Xe	2×10^{15}	1.5	4-7.0	200 ± 40
Kr	2×10^{15}	<1 >1	>12 1.6-3.5	4.7 ± 1.6 527 ± 100
Ti	1×10^{15}	1.2 1.5	4.6-6.0 0-20	84 ± 8 970 ± 70
Fe	$1\text{-}2\times10^{15}$	1.2 1.5	6.5-8.5 0-20	35 ± 15 800 ± 80
Cu	-	1	4-9.5	27 ± 7.5

TABLE II
X-RAY ENVIRONMENT OF THE NIF DEVICE

Target	Laser Energy (MJ)	Pulse Width (ns)	Energy Band (keV)	X-ray Yield (J/sr)
Ar:Xe	0.35	3-5	3-7.0 <3	8.4 ± 0.8 16.8 ± 2.4
Kr:Xe	1.34	14	3.5-7 <3	4.9 ± 0.24 38.4 ± 5.8
Kr	0.75	3-5	>9	1.6 ± 0.1
Mo	1.0	2	17-20	0.7 ± 0.3
Cu	0.5	4	7.5-9.5	1.6 ± 0.47

to block the electromagnetic pulse interference is necessary, which would generate large number of free electrons after X-ray irradiation, thereby exciting an electromagnetic pulse inside the enclosure. The diagnostics working inside this metal shielding cavity should face serious SGEMP interference. The U.S. National Ignition Facility (NIF) performed many measurements and studies of the X-ray environment and the SGEMP. Since 2015, the research team at NIF has been joined with the Sandia National Laboratories (SNL) and the U.K. Atomic Weapons Establishment and successively conducted two series experiments. An X-ray source was used to irradiate SGEMP diagnostic devices at energies of 7 and 13 keV. Accurate and comprehensive test data were obtained. Plans exist to use higher energy lasers and X-rays in subsequent experiments.

II. X-RAY ENVIRONMENT INSIDE THE TARGET CHAMBER

After a laser acts on a solid target, very strong X-ray radiation is generated, most of which are soft X-rays with less than 3 keV in energy, whereas some are K-level emissions in the energy range of 4–15 keV produced by elements in the target with larger proton numbers, such as Ti, Fe, Ge, and Kr [8]. To separately measure the X-rays in different energy bands, NIF and SNL developed HENWAY, DANTE, photoconductive detectors, and a variety of diagnostic instruments [9]. Meanwhile, the Shenguang-III (SG-III) device requires a dynamic response range of 0.1–10 keV to diagnose X-rays and uses an X-ray streak camera connected to the crystal spectrometer to record the time-resolved emission spectra [10]. It is found by both experimental measurements and theoretical calculations that there is a significant correlation between X-ray emission and target temperature; different energy bands corresponded to different optimal targeting temperatures. The temperature of the target is directly affected by the energy density of the incident laser, and the energy density depends on parameters such as the laser energy, pulsewidth, and target density and volume. Because the generation of X-rays after laser targeting is affected by a variety of experimental conditions, the X-ray environment in the target chamber is complex and diverse. In Tables I and II, the X-ray environment in the target chamber with an optimized method for estimated guidance accuracy (OMEGA) device

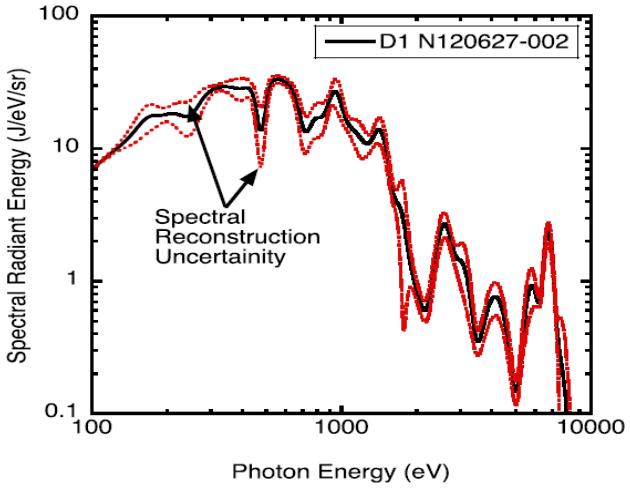

Fig. 2. X-ray spectrum obtained in an experiment [12].

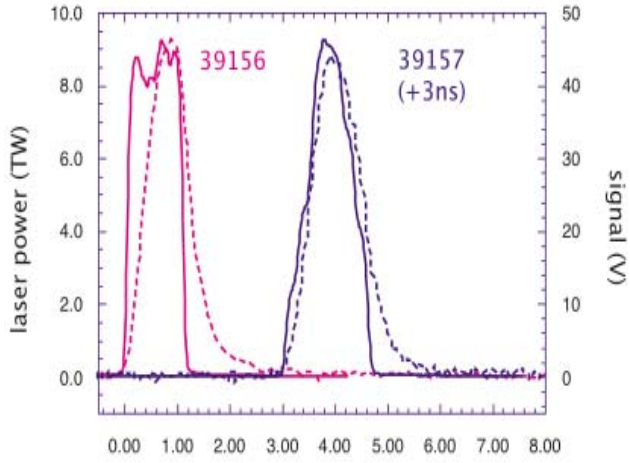

Fig. 3. 4 keV or higher X-ray waveform measured in an experiment (solid lines are the incident laser pulse and dashed–dotted lines are the X-rays) [9].

and an NIF device are summarized based on the experimental measurement results of Fournier [11]. Due to the performance limitations of the X-ray diagnostic equipment, most of the experimental measurement results were data in a certain energy band. Fig. 2 shows a typical X-ray energy spectrum obtained in the NIF device, with a low-energy segment as the main part. Fig. 3 shows the measurement results of the time-domain signal. The waveform of the X-ray level approached

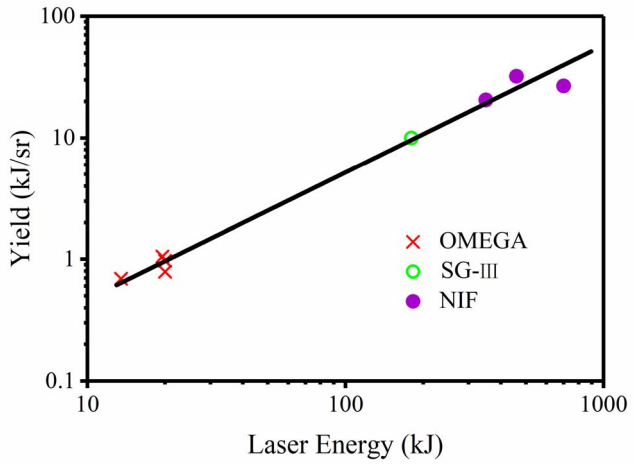

Fig. 4. X-ray environment for different laser energies.

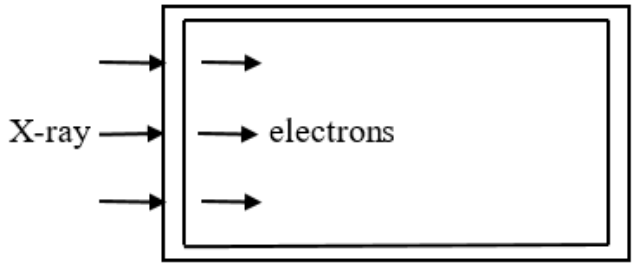

Fig. 5. Physical model of the metal shield cavity outside diagnostics.

a Gaussian distribution in time domain, the pulsewidth was consistent with that of the incident laser, and there was almost no time delay.

In this paper, to facilitate the study of SGEMP caused by X-rays inside the target chamber, the X-ray yields in the full-bandwidth range for different targeting conditions were calculated based on the existing measurement results, with the OMEGA device near 1000 J/sr and the NIF device at approximately 20–30 kJ/sr, as shown in Fig. 4. The SG-III device is a laser ICF device developed and operated by the China Academy of Engineering Physics. Built in 2013, it has a laser output capability with a total energy of 180 kJ and a peak power of 60 TW. Although the X-ray diagnostic data has not yet been published, the laser energy of the SG-III device is between the OMEGA and NIF devices, and the X-ray environment inside the target chamber can be roughly calculated based on Fig. 4 to reach a maximum of more than 10 kJ/sr.

III. Calculation Model and Methods

In this paper, the process of occurrence in the metal shielding cavity is calculated. As shown in Fig. 5, a simplified physical model of the shielding layer is an aluminum cylindrical cavity with a diameter of 20 cm ($d = 20$ cm) and a length of 30 cm ($L = 30$ cm), which is approximated to the size of the actual metal shield cavity. The target chamber is a sphere with a radius of 6 m and diagnostics are usually facing the axis of the target, which is located on the center of the chamber. Considering that the cavity is very small compared to the chamber, it is reasonable to suppose that X-rays uniformly irradiate from one end face of the cylinder along the direction of the axis of symmetry. There are complex interactions between X-ray and materials, such as photoelectric affect, and large number of forward electrons are emitted from the inner surface with the same speed and orientation. Since the X-rays are concentrated in the low-energy spectrum bands, the average energy of the emitted electrons should be several kilo electron volts. By the constraints of computing abilities, we could not handle electrons with a variety of energy, so an average energy is used to replace the complex energy spectrum of electrons.

Due to the symmetry of the cylinder, the model can be simplified into a 2-D cylindrical coordinate system. The finite-difference time-domain (FDTD) method and the particle-in-cell (PIC) method were used in the calculations to solve for the movement of the electrons and the electromagnetic field in the region at any moment. The set of differential forms of Maxwell equations was transformed into the difference schemes of (1) and (2) using the central difference method

$$\boldsymbol{E}^{n+1} = \boldsymbol{E}^{n} + \frac{\Delta t}{\varepsilon}\left(\nabla \times \boldsymbol{H}^{n+\frac{1}{2}} - \boldsymbol{J}^{n+\frac{1}{2}}\right) \tag{1}$$

$$\boldsymbol{H}^{n+\frac{3}{2}} = \boldsymbol{H}^{n+\frac{1}{2}} - \frac{\Delta t}{\mu}(\nabla \times \boldsymbol{E}^{n+1}) \tag{2}$$

where $\boldsymbol{E}$, $\boldsymbol{H}$, and $\boldsymbol{J}$ represent the electromagnetic field strength and current density at the grid node; the superscript of each physical quantity indicates a particular moment; and Δt is the time step. The electrons with similar characteristics were classified as an electron cloud. The electromagnetic field, where the electron cloud is located can be obtained based on the weight of the electron cloud in the grid. Meanwhile; the relativistic effect must be taken into account because, the speed of the electrons is very high. The Boris method was used to obtain the position and velocity of the particle cloud, which divided the movement of the particle cloud into two instances, the two sequential half accelerations caused by the electric fields and the rotation caused by the magnetic field, greatly simplifying the calculation process [13]. Because the space charge was dispersed to the grid node when calculating the current density, the charge distribution produced high-speed nonstatistical jumps, which creates high-frequency noise in the results. To eliminate these unnecessary high-frequency components, the time-biased FDTD method was used for optimization. In the time-biased algorithm, the magnetic field at three consecutive moments was used to calculate the electric field. Besides, a relaxation iteration was introduced to filter the signal using the semiimplicit difference method in the following [14]:

$$\begin{aligned}\boldsymbol{E}^{n+1,i} &= (1-\tau_i)\boldsymbol{E}^{n+1,i-1} + \tau_i \boldsymbol{E}^{n+1,I} + \frac{\tau_i \Delta t}{\varepsilon} \\ &\quad \times \left[\nabla \times \left(\alpha_1 \boldsymbol{H}^{n+\frac{3}{2},i-1} + \alpha_2 \boldsymbol{H}^{n+\frac{1}{2},I} + \alpha_3 \boldsymbol{H}^{n-\frac{1}{2},I}\right) - \boldsymbol{J}^{n+\frac{1}{2}}\right].\end{aligned} \tag{3}$$

where α_1, α_2, and α_3 are the time-biased factors, satisfying $\alpha_1 + \alpha_2 + \alpha_3 = 1$; and τ_i $(i = 1, 2, \ldots, I)$ is the relaxation factor, satisfying $1 = \tau_1 > \tau_2 > \cdots > \tau_I > 0$.

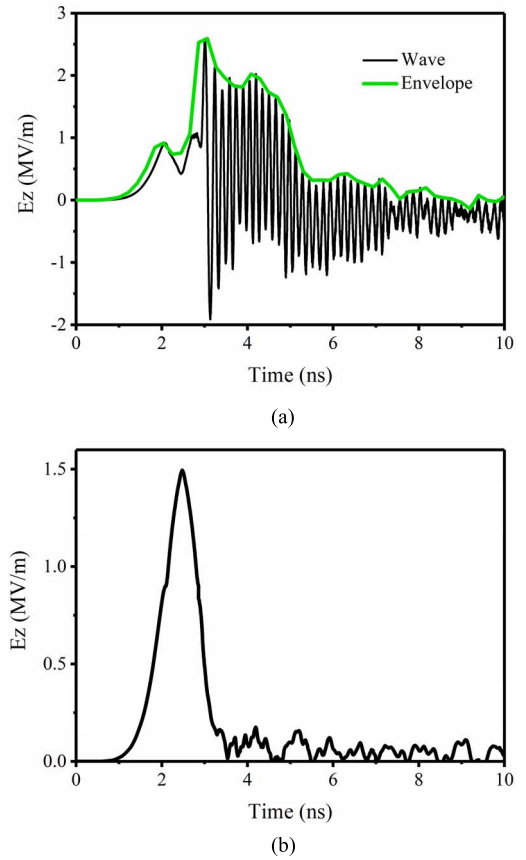

Fig. 6. Time-domain waveforms of the electric field when (a) not including the time-biased algorithm and (b) including the time-biased algorithm.

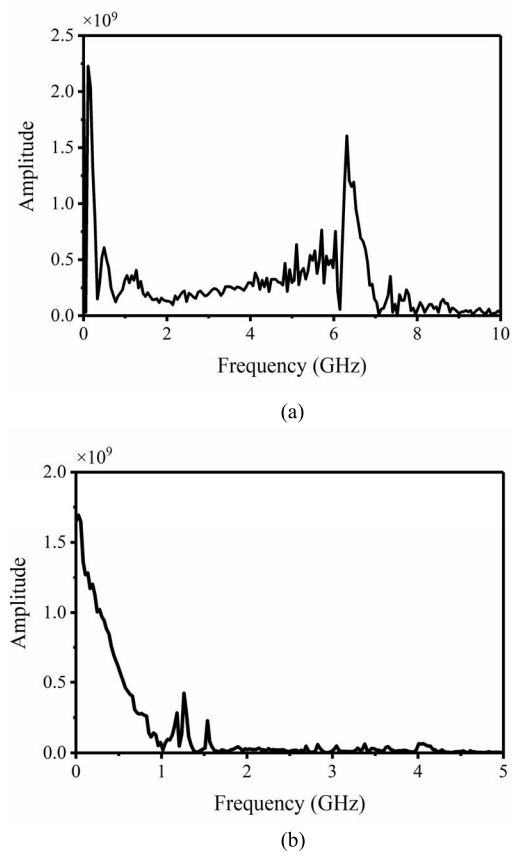

Fig. 7. Frequency spectra of the electric field when (a) not including the time-biased algorithm and (b) including the time-biased algorithm.

Based on the previously mentioned methods, a program can be written to perform a numerical simulation of the process of SGEMP generation.

IV. Numerical Simulation Results and Analysis

The emitted electrons generated after X-ray irradiation on the end face of the cavity can be calculated using the Monte Carlo method. Based on the work of Li *et al.* [15], the total number of electrons could be assumed to be 10^{13} in the simulation. All electrons are emitted perpendicularly from the irradiated end face, and the electron emission time totals 5 ns, the same as the X-ray duration and the pulsewidth of the laser. Since the energy of X-rays is concentrated in the lower part, the average energy of electrons is assumed to be 2 keV. The time-domain waveform of the electromagnetic field strength at the cavity sampling point (a place on the emission surface where radius $r = R/2$) was obtained by calculation, and a frequency spectrum analysis was performed on the results.

A. Comparison on the Optimization Performance of the Time-Biased Algorithm

The electromagnetic field was calculated for two situations: one situation does not include the time-biased algorithm and the other includes the time-biased algorithm. The time-domain waveforms and frequency spectrums of the axial electric field $\boldsymbol{Ez}$ are, as shown in Figs. 6 and 7, respectively. In Fig. 6(a), the green line is the idealized waveform which shows the trend of the field strength, which is consistent with the emission velocity of the electrons, and the blue line is the actual calculation results, in which the electric field strength produced violent fluctuations. In Fig. 7(a), a 6-GHz high-frequency center, which should not exist, appears in the frequency spectrum. Fig. 6(b) shows the results obtained by including the time-biased algorithm, in which the waveform of the electric field became smooth, and in Fig. 7(b), the high-frequency portion of the frequency spectrum disappeared. One can see that the error from the high-frequency jumps of the charge movement cannot be ignored because this behavior causes serious distortion of the electromagnetic field signal and results in inaccurate calculated results. The time-domain waveform of the electric field should be similar to the waveform of emitted electrons, because the SGEMP is excited by emitted electrons. When the electron fluence rate increases, it is the same with the electromagnetic field, and vice versa. Therefore, it is rational that the electromagnetic field calculated in this paper is a pulse lasted for several nanoseconds with a frequency up to a few gigahertz. The waveform that includes the time-biased algorithm for optimization is closer to the SGEMP numerical simulation results by NIF researchers (see Fig. 8, with a maximum electric field strength of about 3 MV/m), which further illustrates the credibility of the results obtained by the time-biased algorithm.

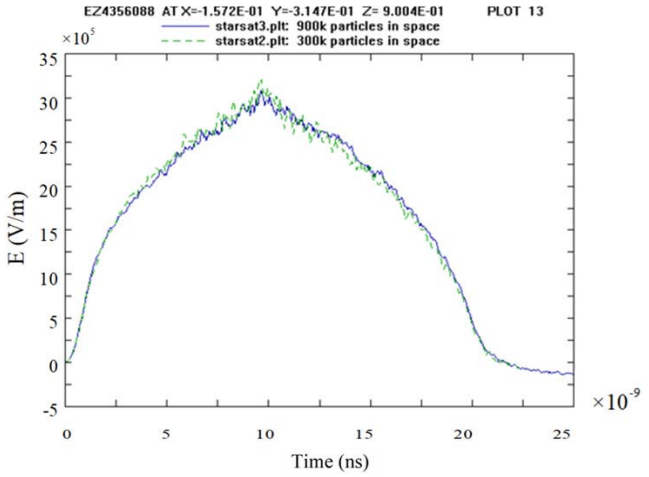

Fig. 8. NIF simulation result of an SGEMP in a satellite [16].

According to the calculation results that include the time-biased algorithm, the peak value of the electric field strength is 1.5 MV/m, the peak value of the magnetic field strength is 277 A/m, and the frequencies of the SGEMP are mainly distributed in the range of less than 1 GHz.

B. Effects of Physical Parameters on the Results

Because the actual radiation environment inside the target chamber of a high-power laser device is very complex, to better simulate the SGEMP response generated in the diagnostic equipment, physical parameters (for the numerical simulation) such as X-ray fluence, pulsewidth, energy spectrum, and model size were changed independently, and their effects on the calculation results were studied.

1) Effect of the X-Ray Fluence: The number of emitted electrons reflects the energy fluence of the incident X-rays. In order to show their relationship more intuitively, we define the electron fluence n with units of electrons per square centimeter. Then, multiple set of calculations were performed to change the number of emitted electrons. The results showed that significant changes appeared in the time-domain waveform of the electromagnetic field inside the cavity. As the electron fluence increased, the time-domain oscillations of the electromagnetic field intensified. Using the magnetic field frequency spectrum shown in Fig. 9, the high-frequency portions gradually increase from Fig 9(a) to (d). When the electron fluence reaches 3.18×10^{10} cm^{-2}, the frequency spectrum is no longer centered in the low frequencies. When the electron fluence reaches 3.18×10^{11} cm^{-2}, the center of the frequency spectrum is increased to 5 GHz. Meanwhile, because of the increase in the electron density, the peak value of the electric field strength continues to rise, but a saturation trend emerges [see Fig. 10(a)]. The emergence of a saturation phenomenon occurs because the field strength increases as the number of electrons increases, and the constraints that the electromagnetic field places on the movement of electrons become stronger, which in turn limits a further increase in the field strength. Fig. 10(b) shows the relationship between the field strength and X-ray fluence that Woods *et al.* obtained and popularized by integrating theory with calculations; their

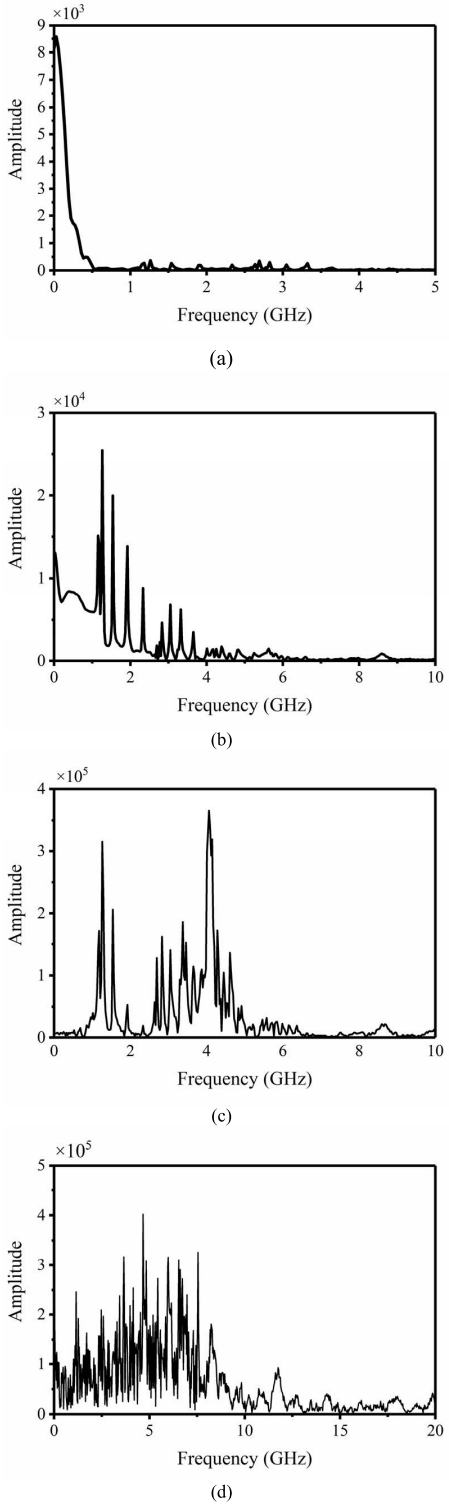

Fig. 9. Frequency spectra of the magnetic field when the electron fluence n is $3.18\times$ (a) 10^8 cm^{-2}, (b) 10^9 cm^{-2}, (c) 10^{10} cm^{-2}, and (d) 10^{11} cm^{-2}.

results are consistent with the trend in the calculated results obtained in this paper. Based on this observation, the peak electric field strength of the SGEMP in the cavity is surmised to not exceed a few MV/m.

2) Effect of the X-Ray Pulsewidth: The duration time of the electrons corresponds to the pulsewidth of the X-ray. In this paper, calculations were performed for pulse widths

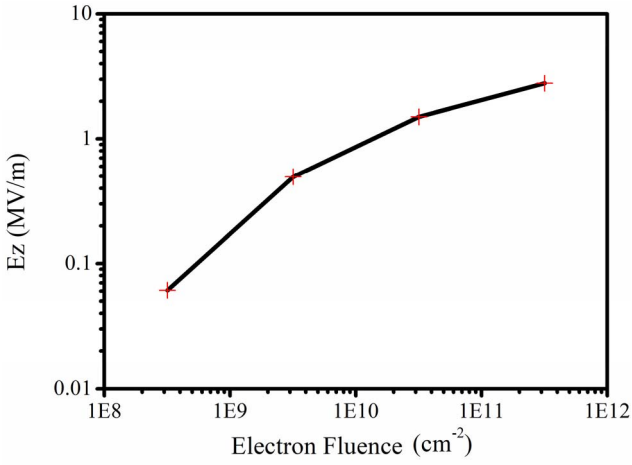

(a)

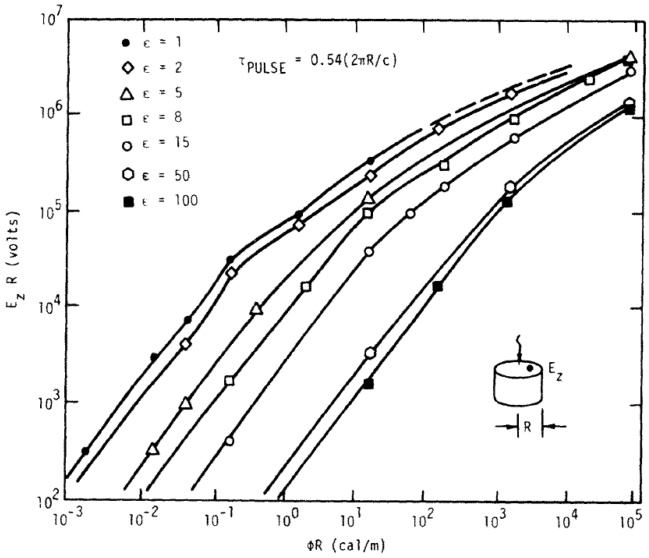

(b)

Fig. 10. Relationship between the peak electric field strength and X-ray fluence (electron fluence) calculated by (a) this paper and (b) Woods and Wenaas [17].

of 1, 5, and 10 ns, and the waveform of the electric field was found to change as the pulsewidth changed, as shown in Fig. 11. This occurs because the electric field strength is affected by the velocity of emitted electron. When electron emission is fast, the charge density is large, the spatial current is high, and the excited electromagnetic field naturally becomes higher. Therefore, the peak value of the electric field and the peak value of emitted electrons appear at almost the exact the same time, and the time-domain waveform is basically consistent with the pulse waveform of the X-ray.

Meanwhile, the shorter the electron emission time is, the greater the emission density is, and the greater the peak strength of the electric field becomes. Fig. 12(a) shows the calculated results of this paper, and Fig. 12(b) shows the relationship between the field strength and X-ray pulsewidth obtained and popularized by Wenaas *et al.* [3] The trends in Fig 12(a) and (b) are consistent.

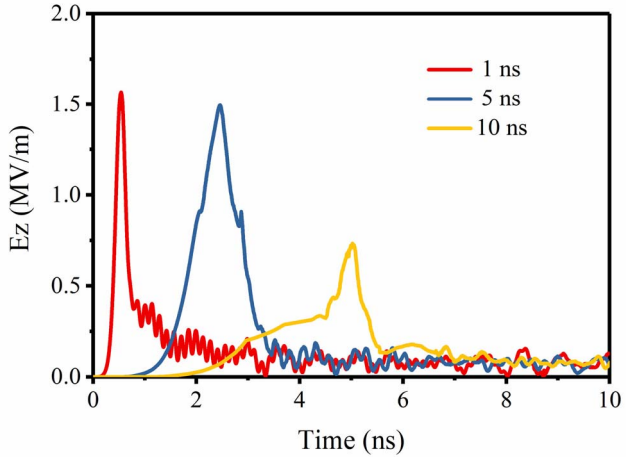

Fig. 11. Electric field waveforms for different pulse widths.

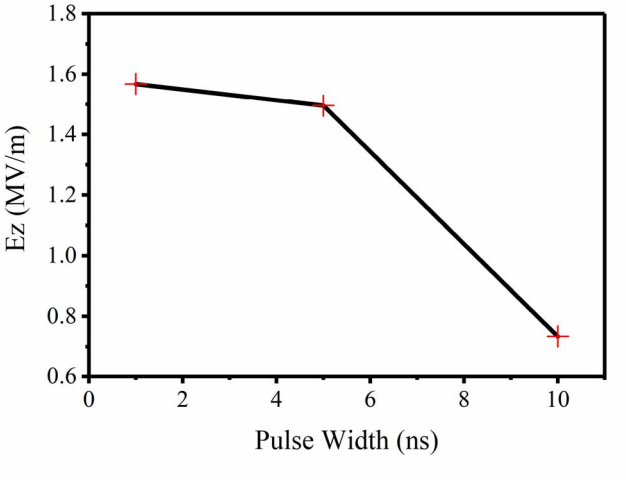

(a)

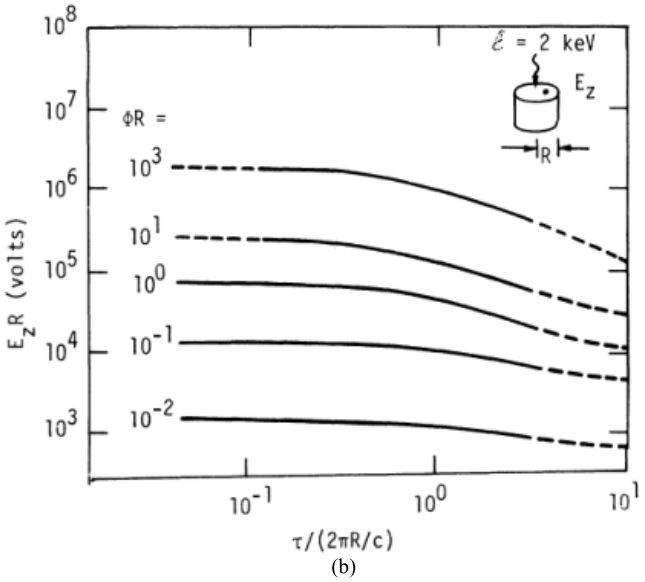

(b)

Fig. 12. Relationship between the peak electric field strength and X-ray pulsewidth calculated by (a) this paper, and (b) Woods and Wenaas [17].

3) Effect of the X-Ray Energy Spectrum: The X-ray energy spectrum determines the energy of the emitted electrons. By changing only the energy of the electrons while the other

TABLE III
RELATIONSHIP BETWEEN THE PEAK ELECTROMAGNETIC FIELD STRENGTH AND X-RAY ENERGY SPECTRUM (THE ENERGY OF THE EMITTED ELECTRONS)

Energy of the electrons (keV)	Electric field strength ($MV \cdot m^{-1}$)	Magnetic field strength ($A \cdot m^{-1}$)
2	1.5	277
20	3.0	290
50	3.2	322

TABLE IV
RELATIONSHIP BETWEEN THE PEAK ELECTROMAGNETIC FIELD STRENGTH AND MODEL SIZE

Radius (cm)	5	10	20	50
Electric field strength (MV/m)	1.47	1.50	0.67	0.03

conditions remained unchanged, the calculations showed that there was almost no change in the time-domain waveform and frequency characteristics of the electromagnetic field, whereas there was only a slight increase in the peak strength. Table III shows changes in the peak values of the electric field strength and the magnetic field strength. The higher the energy of the electrons is, the greater the velocity is, and the greater the excited electromagnetic field strength is, but the effect is not significant and would not cause a significant change in the frequency spectrum. In actuality, when the X-ray fluence remains unchanged, higher energy in individual electrons means fewer total electrons, which would weaken the effect of the energy spectrum changes on the electromagnetic field. Moreover, the peak value of the electromagnetic field at this time is very large and would soon reach saturation, further restricting the effect caused by an increase in the energy of the electrons.

4) Effect of the Model Size: Since the diagnostic equipment in use in the target chamber differs in size, there is a need to study the SGEMP interference in the cavity for different spatial sizes. The calculation results showed that when changing the radius and length of the cylindrical model, the time-domain waveform and the frequency spectrum of the electromagnetic field are fundamentally unchanged, while the peak strength does change, as shown in Table IV. Because the total number of emitted electrons does not change in the calculations, a larger model results in a smaller emission density of electrons, and a smaller peak strength. In actuality, the X-ray has a uniform incidence and the area of the irradiated end face is proportional to the number of emitted electrons; therefore, the size of the equipment and the number of emitted electrons would change synchronously, and the generated electromagnetic field should be the same.

C. Predictions on the SGEMP in the Target Chamber of the SG-III Device

The results of numerical simulations and existing international studies on SGEMP are in agreement to a great extent, indicating that the calculated results are credible and can be used as a basis to predict the SGEMP in the target chamber of the SG-III device. The target chamber of the SG-III device is 6 m in diameter and contains six bundles, totally48 beams of a frequency-tripled Nd:glass pulsed laser, which has the capability of shaping the pulse to within a 10 ns pulsewidth. When the SG-III device emits a laser with energy of 180 kJ and a pulsewidth of 10 ns, the strength of the X-rays in the target chamber can reach more than 10 kJ/sr, and the SGEMP peak field strength that would be generated under these conditions can be predicted to approximately be 0.75 MV/m.

V. CONCLUSION

In laser-inertial confinement devices, SGEMP could cause serious electromagnetic interference to diagnostic equipment, which indicates that effective radiation shielding should be taken to protect the diagnostics from interference. Based on a cylindrical cavity model, time-biased FDTD and PIC methods were used in this paper to compile a 2-DSGEMP calculation program. Survey results of the X-ray environment in a target chamber were used as the foundation for conducting a series of numerical simulations.

Through a comparative analysis of the calculated results in this paper, the effects of the incident X-ray fluence, pulsewidth, energy spectrum distribution, and spatial size of the model on the strength of the SGEMP were explored. When the X-ray fluence raises, the frequency of electromagnetic field would increase significantly and the peak value would also continue to rise. When the X-ray pulsewidth increases, the waveform of SGEMP would broaden, the strength of electromagnetic field would decrease, and the appearance of the peak would be delayed. When the X-ray energy is enhanced, the strength of SGEMP would increase. While the effect of the X-ray fluence and pulsewidth is found to be significant, the X-ray energy seems to have little influence on the SGEMP. Besides, it is interesting to figure out that when the model becomes bigger, the strength of SGEMP would decrease.

Finally, it was predicted that the SGEMP interference in the target chamber of the SG-III device should approximately be 0.75 MV/m.

REFERENCES

[1] K. Zhou, Y. Wang, and J. Deng, "Research for SGEMP synthesize response of typical-cable bind," in *Proc. China Nucl. Sci. Technol. Progr. Rep.*, Harbin, China, 2013, p. 5.

[2] Y. Liu, "Study on SGEMP-simulated experiment," in *Proc. 9th Nat. Conf. Nucl. Electron. Nucl. Detection Technol.*, Dalian, China, 1998, p. 3.

[3] E. P. Wenaas, S. Rogers, and A. J. Woods, "Sensitivity of SGEMP response to input parameters," *IEEE Trans. Nucl. Sci.*, vol. NS-22, no. 6, pp. 2362–2367, Dec. 1975.

[4] O. Lopez and W. F. Rich, "Dynamic internal electromagnetic pulse calculations in three spatial dimensions," *IEEE Trans. Nucl. Sci.*, vol. NS-20, no. 6, pp. 14–19, Dec. 1973.

[5] A. J. Woods and E. P. Wenaas, "Precharging effects on the SGEMP response," *IEEE Trans. Nucl. Sci.*, vol. NS-25, no. 6, pp. 1365–1369, Dec. 1978.

[6] H. Zhou, H. Guo, B. Li, Y. Chen, and D. Chang, "Response of metal shell and cables to system generated electromagnetic pulse effects," *High Power Laser Particle Beams*, vol. 16, no. 5, pp. 645–648, 2004.

[7] H. Zhou, L. Baozhong, W. Lijun, and C. Yusheng, "The calculation of SGEMP response in various ranges of X-ray fluence," *Chin. J. Comput. Phys.*, vol. 16. no. 2, pp. 47–51, 1999.
[8] F. Pérez *et al.*, "Bright X-ray sources from laser irradiation of foams with high concentration of Ti," *Phys. Plasmas*, vol. 21, no. 2, p. 023102, 2014.
[9] K. B. Fournier *et al.*, "Absolute X-ray yields from laser-irradiated germanium-doped low-density aerogels," *Phys. Plasmas*, vol. 16, no. 5, p. 052703, 2009.
[10] X. Hu, S. Liu, Y. Ding, Q. Yang, J. Tian, and X. He, "Design of SG-III X-ray streak camera," *Acta Opt. Sinica*, no. 10, pp. 2871–2875, 2009.
[11] K. B. Fournier, "NIF and OMEGA X-ray environments summary," Tech. Rep., 2015.
[12] M. J. May *et al.*, "Bright X-ray stainless steel k-shell source development at the national ignition facility," *Phys. Plasmas*, vol. 22, no. 6, p. 063305, 2015.
[13] J. Zhou, "Electromagnetic particle-in-cell simulation method and its applications," to be published.
[14] J. Zhou, D. Zhu, D. Liu, and S. Liu, "Time-biased FDTD method for particle-in-cell simulation," *Chin. J. Comput. Phys.*, vol. 24, no. 5, pp. 566–572, 2007.
[15] J. Li, Y. Cheng, W. Wu, and H. Zhou, "Software for calculating system generated electromagnetic pulse in cylindrical cavity," in *Proc. Nat. Conf. Nucl. Electron. Nucl. Detection Technol.*, Ürümqi, China, 2008.
[16] M. Bland, D. Walters, and J. Wondra, "Graphical interface for the physics-based generation of inputs to 3D MEEC SGEMP and SREMP simulations," Office Sci. Tech. Inf., Oak Ridge, TN, USA, Tech. Rep., 1998.
[17] A. J. Woods and E. P. Wenaas, "Scaling laws for SGEMP," *IEEE Trans. Nucl. Sci.*, vol. NS-23, no. 6, pp. 1903–1908, Dec. 1976.